



# CHORUS

This is the accepted manuscript made available via CHORUS. The article has been published as:

## Evolution of the electronic structure in ultrathin Bi(111) films

Lin Miao, Meng-Yu Yao, Wenmei Ming, Fengfeng Zhu, C. Q. Han, Z. F. Wang, D. D. Guan, C. L. Gao, Canhua Liu, Feng Liu, Dong Qian, and Jin-Feng Jia

Phys. Rev. B **91**, 205414 — Published 12 May 2015

DOI: [10.1103/PhysRevB.91.205414](https://doi.org/10.1103/PhysRevB.91.205414)

# Evolution of the electronic structure in ultrathin Bi(111) films

Lin Miao,<sup>1</sup> Meng-Yu Yao,<sup>1</sup> Wenmei Ming,<sup>2</sup> Fengfeng Zhu,<sup>1</sup> C. Q. Han,<sup>1</sup> Z. F. Wang,<sup>2</sup> D. D. Guan,<sup>1,3</sup> C. L. Gao,<sup>1,3</sup> Canhua Liu,<sup>1,3</sup> Feng Liu,<sup>2</sup> Dong Qian,<sup>1,3,\*</sup> and Jin-Feng Jia<sup>1,3</sup>

<sup>1</sup>Key Laboratory of Artificial Structures and Quantum Control (Ministry of Education), Department of Physics and Astronomy, Shanghai Jiao Tong University, Shanghai 200240, China

<sup>2</sup>Department of Materials Science and Engineering, University of Utah, Salt Lake City, UT 84112, USA

<sup>3</sup>Collaborative Innovation Center of Advanced Microstructures, Nanjing 210093, China

By combining angle-resolved photoemission spectroscopy (ARPES) and first-principle calculations, we systematically studied the electronic structures of ultrathin Bi(111) films ( $\leq 5$  bilayers) epitaxially grown on Bi<sub>2</sub>Te<sub>3</sub>. High-resolution low-energy band dispersions and Fermi surfaces of ultrathin Bi(111)/Bi<sub>2</sub>Te<sub>3</sub> films as a function of thickness were experimentally determined. Our results also indicate that the electronic structures of epitaxial Bi films are strongly influenced by the substrate compared with free-standing films. The substrate effects mainly include two aspects. First, the in-plane lattice constant of Bi(111) films is compressed, which increases the bandwidth of the surface-state-like bands. Furthermore, the band dispersion near  $\bar{\Gamma}$  point is significantly modified as well. Second, there exists a strong hybridization at the Bi /Bi<sub>2</sub>Te<sub>3</sub> interface, and the hybridization effects spatially extend to three Bi bilayers.

Bismuth (Bi) is a heavy element and its electronic structures are highly influenced by the spin-orbit coupling. Bulk Bi crystal is famous for its novel spin-split surface states caused by the large spin-orbit coupling<sup>1-4</sup>. Along  $\langle 111 \rangle$  direction, the stable and smallest unit of Bi is the bilayer (BL) structure<sup>1</sup>. Theoretically, these surface states show very interesting behavior in ultrathin films<sup>5</sup>. In theory, ultrathin free-standing Bi(111) BLs exhibit a semiconductor to semi-metal transition with the increase of thickness and the crossover thickness is 4 or 5 BLs depending on the strength of inter-bilayer coupling<sup>5,6</sup>. Theoretical calculations predicted that ultrathin semiconducting Bi(111) BLs were two dimensional (2D) topological insulators (TI)<sup>6-8</sup>. However, such kind of free-standing Bi(111) BLs have not been realized experimentally. It is only very recently that Bi(111) films were successfully grown on Bi<sub>2</sub>Te<sub>3</sub>(111) (or Bi<sub>2</sub>Se<sub>3</sub>) substrate from single BL to multi BLs<sup>9-15</sup>, which made the experimental studies of the electronic structures of ultrathin Bi(111) films possible. Bi<sub>2</sub>Te<sub>3</sub> is a 3D TI with topological Dirac-cone like surface states<sup>16</sup>. Recently, electronic structures of 1-BL Bi(111)/Bi<sub>2</sub>Te<sub>3</sub> were studied by ARPES and density functional theory (DFT) calculations<sup>9-12</sup>. Though the band structures are very different from free-standing 1-BL Bi(111) and strong hybridization between Bi and Bi<sub>2</sub>Te<sub>3</sub>'s surface states occurs, the non-trivial topological properties were confirmed in 1-BL Bi(111)/Bi<sub>2</sub>Te<sub>3</sub> by scanning tunneling microscopy and ARPES<sup>9,10,13,17</sup>. However, no high-resolution band structures have been reported on multi-BL Bi(111)/Bi<sub>2</sub>Te<sub>3</sub> films. It is important to know how the electronic structures changes from 1-BL to multi-BL in Bi/Bi<sub>2</sub>Te<sub>3</sub> system. It is also very interesting to know the interaction or hybridization between Bi and Bi<sub>2</sub>Te<sub>3</sub> beyond single-BL Bi(111) films. By combining ARPES and DFT calculations, in this paper we studied the electronic structures of Bi(111) films ( $\leq 5$  BLs) on Bi<sub>2</sub>Te<sub>3</sub> substrate. The energy bands and Fermi surface

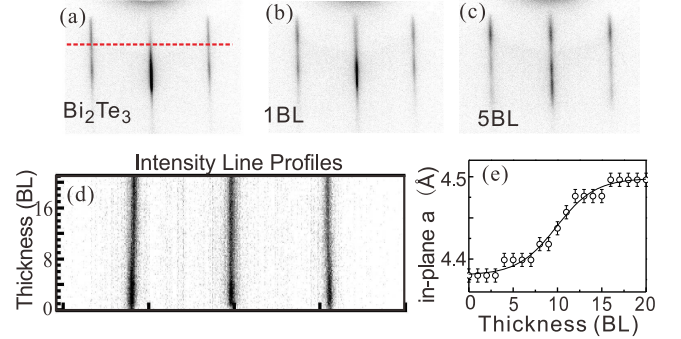


FIG. 1. RHEED patterns of (a) 40 QLs Bi<sub>2</sub>Te<sub>3</sub> grown on Si(111), (b) 1-BL Bi(111) and (c) 5-BL Bi(111) films on Bi<sub>2</sub>Te<sub>3</sub>. (d) RHEED intensity line profiles with the increase of film thickness. The position where the intensity line profile was taken is marked by red dashed line in (a). (e) In-plane lattice constant of Bi films as a function of film thickness. Solid line is for eye-guide.

(FS) topology were experimentally determined. The effects of substrate were discussed in detail. Surface-states-like states in Bi(111) are modified due to the stress of Bi/Bi<sub>2</sub>Te<sub>3</sub> interface. Except single-BL Bi(111), there is no hybridization between Bi and the Dirac-cone surface states of Bi<sub>2</sub>Te<sub>3</sub>. Hybridization between Bi and Bi<sub>2</sub>Te<sub>3</sub>'s bulk bands exists within 3 BLs from the interface.

Bi<sub>2</sub>Te<sub>3</sub>(111) films of 40 quintuple layers (QLs) were grown by MBE on Si(111) wafer. Bi(111) films were grown on Bi<sub>2</sub>Te<sub>3</sub> at 250 K. ARPES measurements were carried out with helium discharge lamp (He-I 21.2 eV) using Scienta analyzer and in Advanced Light source beamlines 4.0.1 and 12.0.1. Energy resolution is better than 25 meV and angular resolution is better than 1% of Brillouin zone (BZ). The sample temperature was kept at 100K during measurements. DFT calculations were carried out in the framework of generalized gradient approx-

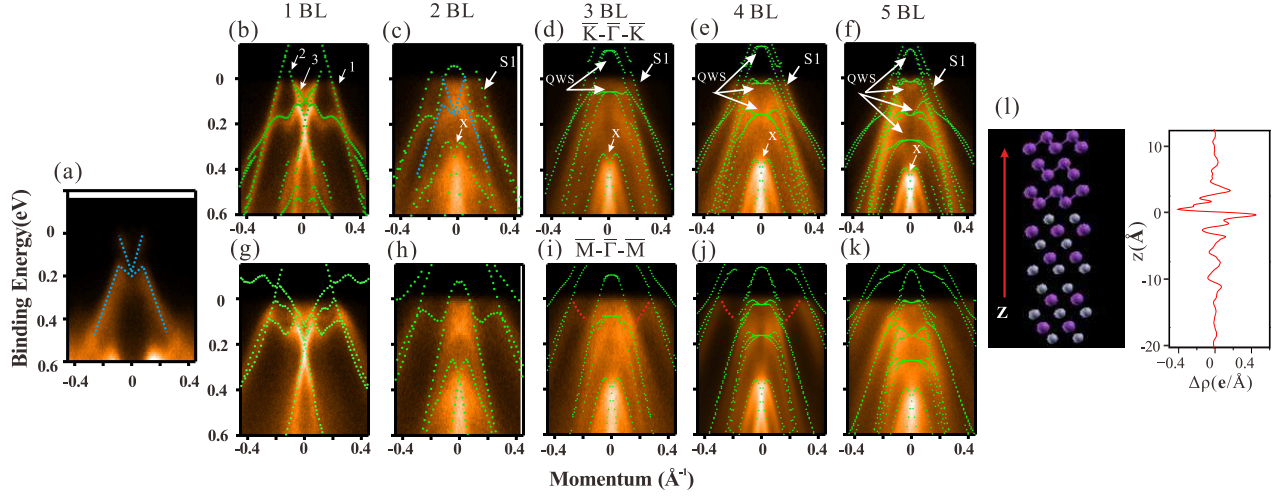


FIG. 2. (a) ARPES spectra of 40QLs Bi<sub>2</sub>Te<sub>3</sub>(111) film along  $\bar{K}-\bar{\Gamma}-\bar{K}$  direction. Blue dashed lines mark the surface states and valence bands. (b-f) ARPES spectra of 1-BL Bi(111) to 5-BL Bi(111) films along  $\bar{K}-\bar{\Gamma}-\bar{K}$  directions. (g-k) ARPES spectra of 1-BL Bi(111) to 5-BL Bi(111) films along  $\bar{M}-\bar{\Gamma}-\bar{M}$  direction. The green dashed lines are the calculated spectra from top 2 Bi BLs. White arrows in (b) and (g) mark the bands that cross the Fermi level to form Fermi surface. Blue dashed lines in (c) are from (a). Quantum well states are marked by "QWS". Outmost hole-like band and Rashba-type splitting bands are marked by "S1" and "X". Red dotted lines in (i) and (j) present the hybridization bands. (l) The side view of 3-BL Bi(111) on Bi<sub>2</sub>Te<sub>3</sub> and differential charge density near interface. 1 QL is 1 nm and 1 BL is 0.4 nm.  $Z=0$  is the interface.

imation with Perdew-Burke-Ernzerhof functional using the VASP package<sup>18</sup>. The in-plane lattice constant of Bi(111) films was strained to match the substrate lattice parameter. All calculations were performed with a plane-wave cutoff of 600 eV on an  $11 \times 11 \times 1$  Monkhorst-pack k-point mesh. The substrate was modeled by a slab of 6-QL Bi<sub>2</sub>Te<sub>3</sub>, and the vacuum layers were over 20Å thick to ensure decoupling between neighboring slabs. During structural relaxation, atoms in the lower 4-QL substrate were fixed in their respective bulk positions, and Bi BLs and upper 2-QL of the substrate are allowed to relax until the forces were smaller than 0.01 eV/Å.

The sharp line-like reflection high-energy electron diffraction (RHEED) pattern of Bi<sub>2</sub>Te<sub>3</sub> (Fig. 1(a)) indicates a high-crystalline-quality and flat surface. After the Bi deposition (Fig. 1(b) and 1(c)), the line-like RHEED pattern remains. Layer-by-layer growth mode of Bi on Bi<sub>2</sub>Te<sub>3</sub> was observed by RHEED intensity oscillations as reported previously<sup>12</sup>. The distance between two adjacent lines in the RHEED pattern is inversely proportional to in-plane lattice constant. Fig. 1(d) shows the intensity line profiles (red dotted line Fig. 1(a)) with the increase of Bi thickness. Zero-BL refers to the substrate. By tracing the relative change of peak position in Fig. 1(d), we obtained the in-plane lattice constant of Bi ( $a_{Bi}$ ) as a function of thickness (Fig. 1(e)). Thinner than 3 BLs,  $a_{Bi}$  is nearly the same as the substrate (4.38 Å) within the experimental uncertainty. Then  $a_{Bi}$  increases slightly. Thicker than  $\sim 7$  BLs,  $a_{Bi}$  begins to increase quickly until about 15 BLs. After 15 BLs,  $a_{Bi}$  reaches  $\sim 4.5$  Å that is very close to bulk Bi (4.54 Å). Smooth change of  $a_{Bi}$  and lack of dislocations confirmed by STM indicate that strain in the films is very likely

released through continuous increase of  $a_{Bi}$  in each BL.

Figure 2 presents the ARPES spectra along high-symmetry directions. Spectra of Bi<sub>2</sub>Te<sub>3</sub> are shown in Fig. 2(a). Blue dotted lines mark the Dirac-cone like surface states and valence bands of Bi<sub>2</sub>Te<sub>3</sub>. In Fig. 2(b) - 2(k), green dotted lines are the theoretical bands (Note: though DFT calculations we plotted did not include the spectra of substrate. The thickness of 1-BL is about 0.4 nm. Because ARPES probing depth is about 1 nm, we only plotted contributions from top 2-BL Bi for 2 - 5 BLs Bi films to compare with experimental spectra). According to previous calculations, free-standing Bi(111) films ( $a_{Bi}=4.54$  Å) thinner than 5 BLs are semiconductors<sup>6</sup> and strained free-standing Bi(111) films ( $a_{Bi}=4.38$  Å) are semiconductors below 2 BLs<sup>13</sup>. Experimentally, we found that the Fermi level did not locate in the energy gap for all films. There is charge transfer between the films and the substrate. The Te atoms on the Bi<sub>2</sub>Te<sub>3</sub> surface would have a larger electronegativity than the Bi. This charge transfer phenomenon was confirmed by DFT calculation. In Fig. 2(l), we show the differential charge density, defined as  $\Delta\rho = \rho_{Bi+Bi_2Te_3} - \rho_{Bi} - \rho_{Bi_2Te_3}$ , for 3-BL Bi(111)/Bi<sub>2</sub>Te<sub>3</sub>. Substantial charge transfer at the interface occurs.  $\Delta\rho$  is negative in Bi side and positive in Bi<sub>2</sub>Te<sub>3</sub> side, which means that electrons are transferred from Bi to Bi<sub>2</sub>Te<sub>3</sub>.

ARPES spectra of 1-BL Bi (Fig. 2(b)) are very different from other thicknesses. The agreement between experimental spectra and DFT calculations is very good for 1-BL film. Since we have discussed 1-BL results in our previous reports<sup>12,14</sup>, we will not discuss it in detail here. The main conclusions on 1-BL film are that there is

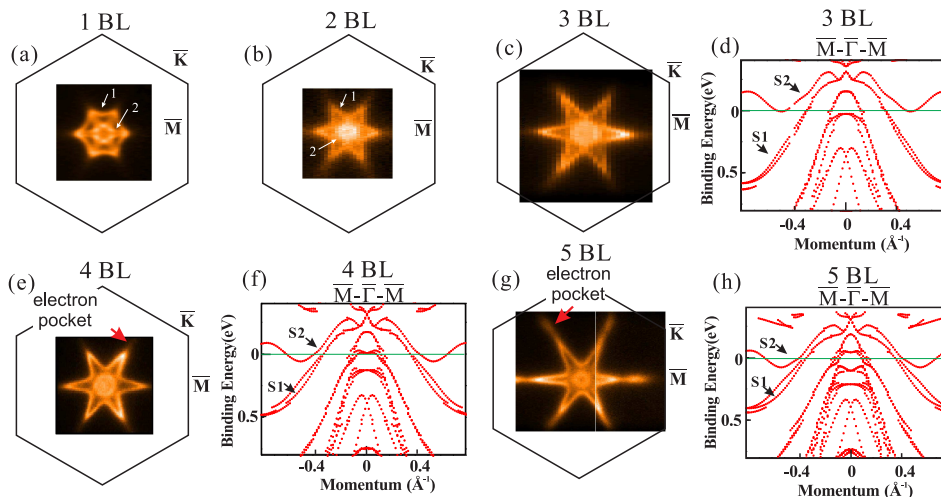


FIG. 3. (a) Fermi surface of 1-BL and (b) 2-BL Bi(111) films. white arrows mark the outer and inner Fermi surface sheets. (c) Experimental FS and (d) The calculated bands along the  $\overline{M}-\overline{\Gamma}-\overline{M}$  direction of 3-BL Bi(111)/Bi<sub>2</sub>Te<sub>3</sub> film. (e) Experimental FS and (f) The calculated bands along the  $\overline{M}-\overline{\Gamma}-\overline{M}$  direction of 4-BL Bi(111)/Bi<sub>2</sub>Te<sub>3</sub> film. (g) Experimental FS and (h) The calculated bands along the  $\overline{M}-\overline{\Gamma}-\overline{M}$  direction of 5-BL Bi(111)/Bi<sub>2</sub>Te<sub>3</sub> film. Calculated bands only include the contributions from top 2-BL Bi. The Fermi levels (green lines) in calculated bands are adjusted based on the size of FS originate from S1 band.

strong hybridization between Bi and Bi<sub>2</sub>Te<sub>3</sub> due to close energy proximity, which results in appearance of Dirac-cone-like states in Bi layers<sup>12</sup>. No strong chemical bond exists in Bi/Bi<sub>2</sub>Te<sub>3</sub> system<sup>11,12</sup>. In Fig. 2(c), for 2-BL film, the calculated spectra agree with the experimental spectra very well except some spectral features near  $\overline{\Gamma}$  point. We overlaid the bands of Bi<sub>2</sub>Te<sub>3</sub> substrate from Fig. 2(a) in Fig. 2(c) (blue dotted lines). Actually, the bands from Bi<sub>2</sub>Te<sub>3</sub> fit those spectra very well. For 3 to 5-BL films, no clear signals from the substrate were observed and the calculated spectra of top 2-BL Bi are in good agreement with the experimental results along  $\overline{K}-\overline{\Gamma}-\overline{K}$  direction. There are some minor discrepancies along  $\overline{M}-\overline{\Gamma}-\overline{M}$  direction (we will discuss it later in Fig. 3 and Fig. 4). In Fig. 2(d) - 2(f), two features do not change dramatically with the increase of film thickness. First, the outmost hole-like band (labeled by "S1") are similar. S1 band has larger Fermi vector ( $k_F$ ) along  $\overline{M}-\overline{\Gamma}-\overline{M}$  than along  $\overline{K}-\overline{\Gamma}-\overline{K}$ . According to previous calculations<sup>5</sup>, S1 band is "surface state" like. It is not real surface state but will develop to real surface state in very thick films or bulk Bi. Second, there are hole-like bands with Rashba-type splitting centered at  $\sim 0.5$  eV below Fermi energy (labeled by "X"). Between S1-band and X-band, we observed more and more bands with the increase of film thickness. Consistent with previous calculations, those bands are quantum well states of Bi valence bands (labeled by "QWS")<sup>5</sup>.

Figure 3 shows the Fermi surfaces of Bi films and calculated bands along  $\overline{M}-\overline{\Gamma}-\overline{M}$ . Fig. 3(a) and 3(b) show the measured FS of 1 and 2-BL films. The FS of 1-BL

film consists of two Fermi sheets. The outer big hexagonal sheet originates from the outmost hole-like band (labeled by "1" in Fig. 2(b)). The inner FS is a small circle with six horns along  $\overline{\Gamma}-\overline{M}$  directions. The inner FS is an electron pocket originated from band "2", band "3" (labeled in Fig. 2(b)). For 2-BL film, FS also consists of two sheets. Different from 1-BL film, both sheets are hole pockets. The outer FS sheet is hexagram-like. The inner small sheet is rounded. FS of 3-BL film (Fig. 3(c)) shows two hole pockets, which is similar to 2-BL film. The outer FS is related to S1 band and the inner circle is related to QWS. According to DFT calculations (Fig. 3(d)), there are two surface-state-like bands (labeled by "S1" and "S2") near Fermi level. In bulk Bi(111), S1 and S2 are two real surface states caused by Rashba-type spin-orbital splitting. In free-standing thin films ( $a_{Bi}=4.54$  or  $4.38$  Å), due to the interaction between upper and bottom surfaces, the degeneracy of S1 and S2 bands at  $\overline{\Gamma}$  and  $\overline{M}$  points is removed<sup>5,13</sup>. Especially, there opens a large energy gap at  $\overline{M}$  point. Different from free-standing film, our calculations shows that the splitting between S1 and S2 bands is nearly zero at  $\overline{\Gamma}$  point for Bi/Bi<sub>2</sub>Te<sub>3</sub>. Usually, the calculated Fermi level is not exactly the same as experiments, so we have to adjust the Fermi level of the calculated bands to compare with experiments. Based on the experimental  $k_F$ , the determined Fermi level of 3-BL Bi (green line) cuts through the bottom of S2 band (Fig. 3(d)), which results in a tiny electron pocket. In contrast, no electron pocket was observed along  $\overline{\Gamma}-\overline{M}$  direction in 3-BL film. In Fig. 3(f) and 3(h), with the increase of Bi thickness, the energy gap between S1 and S2 bands at  $\overline{M}$



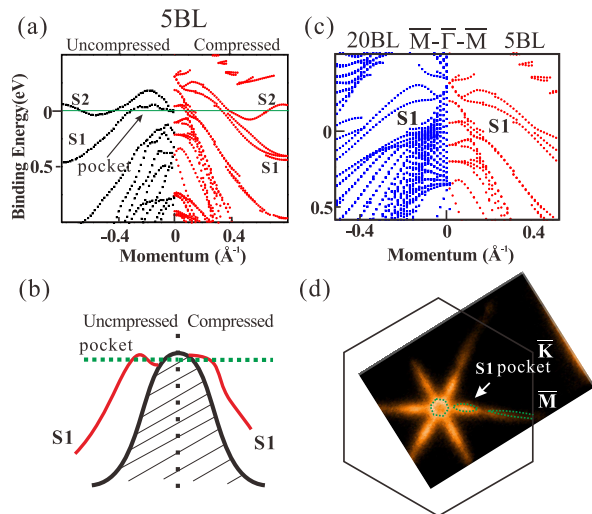


FIG. 4. (a) Calculated band structures of 5-BL Bi(111) with uncompressed in-plane lattice constant ( $a_{Bi}=4.54$  Å) (from reference [5]) and of 5-BL Bi(111)/Bi<sub>2</sub>Te<sub>3</sub> with compressed in-plane lattice constant ( $a_{Bi}=4.38$  Å) along the  $\bar{\Gamma}-\bar{M}$  direction. (b) The sketch of the strain effect on S1 band. (c) Calculated band structures near  $\bar{\Gamma}$  point of 20-BL and 5-BL Bi(111)/Bi<sub>2</sub>Te<sub>3</sub> with compressed in-plane lattice constant ( $a_{Bi}=4.38$  Å). (d) Experimental FS of 20-BL Bi(111)/Bi<sub>2</sub>Te<sub>3</sub> with ( $a_{Bi}=4.5$  Å).

point decreases and the size of electron pocket related to S2 band increases. ARPES spectra show the same trend, though the observed electron pockets are smaller than calculations.

We believe that the discrepancy between experiments and calculations along  $\bar{\Gamma}-\bar{M}$  direction is related to  $a_{Bi}$ . In our DFT calculations, we assumed that  $a_{Bi}$  of Bi films is uniform and the same as substrate. In real films, it is not. Each Bi BL can have different  $a_{Bi}$  that is larger than the substrate. S1 and S2 bands are sensitive to the lattice constant. To illustrate the how the in-plane lattice compression affect S1 and S2 bands' dispersion, we compared the DFT results of uncompressed ( $a_{Bi}=4.54$  Å) and compressed ( $a_{Bi}=4.38$  Å) 5-BL Bi(111) in Fig. 4(a). There are two main differences between two cases. First, S2 band is much flatter in uncompressed film. As Fig. 4(a) shows, the electron pocket related to S2 becomes smaller when  $a_{Bi}$  is larger, which explains the discrepancy between experiments and DFT calculations along  $\bar{\Gamma}-\bar{M}$  direction. Second, the dispersion of S1 band near  $\bar{\Gamma}$  point changes a lot. As illustrated in Fig. 4(b), S1 crosses  $E_F$  twice in uncompressed film and once in compressed film. This effect is thickness independent if  $a_{Bi}$  does not change. We did DFT calculations on 20-BL film with  $a_{Bi}=4.38$  Å. In Fig. 4(c), S1 bands in 5 BLs and 20 BLs Bi(111) ( $a_{Bi}=4.38$  Å) have the similar dispersion relations near  $\bar{\Gamma}$  point. Experimentally, we also measured FS of 20-BL Bi/Bi<sub>2</sub>Te<sub>3</sub> ( $a_{Bi}=4.5$  Å). Because of the large  $a_{Bi}$ , the measured FS is the same as bulk Bi(111)<sup>1</sup> (Fig. 4(d)). S1 crosses  $E_F$  twice to form six hole pockets.

Finally, we discuss the hybridization effect between Bi and the substrate. Figure 5 shows the layer dependence of the projected spectra in DFT calculations for 4-BL Bi/Bi<sub>2</sub>Te<sub>3</sub>. Films of other thicknesses have similar results (except 1-BL). Fig. 5(b) and 5(g) present the spectra from the top 1-BL (4th BL from the interface) Bi along  $\bar{\Gamma}-\bar{M}$  and  $\bar{\Gamma}-\bar{K}$  direction, respectively. S1 and S2 have large spectral weight in the top 1-BL. In Fig. 5(b), there is a large energy gap of about 0.4 eV at  $\bar{\Gamma}$  point. In free-standing films, similar gap exists<sup>5</sup>. Away from  $\bar{\Gamma}$  point, there are some weak spectra coming from QWS of Bi conduction bands. Fig. 5(c) and 5(h) present the spectra from the bottom 1-BL (1st BL from the interface) Bi. The band "X" is very strong in top 1-BL but has no spectral weight in bottom 1-BL. Very different from top 1-BL, in Fig. 5(c), strong electron-like bands (labeled by "H1") exist within the gap. In Fig. 5(h), other electron-like spectra also exist in the valence bands (labeled by "H2"). H1 and H2 bands are caused by the hybridization between Bi and Bi<sub>2</sub>Te<sub>3</sub>. According to DFT, H1 bands can extend to the third BL from the Bi/Bi<sub>2</sub>Te<sub>3</sub> interface. Fig. 5(d) presents the total spectra from the top 2BLs of Bi. H1 bands already exist in the gap, though the spectral weight is weak. There is no H2 bands in the top 2BLs. Because H1 bands are above Fermi level, we can only detect H2 bands experimentally. In Fig. 2(j), on 4-BL Bi, we did observe spectra of weak intensity (guided by red dotted lines) from H2. In Fig. 2(k), on 5-BL Bi, no sign of H2 bands is resolvable. Considering our ARPES depth length ( $\sim 1\text{nm} \approx 3\text{BLs}$ ), we think H2 states should locate 2 or 3 BLs below the surface for 4-BL film as DFT suggested. By combining DFT and ARPES results, we suggest that the hybridization effects can extend spatially to the third Bi BL (H1 bands) from the interface. Fig. 5(e) presents the total spectra of 4-BL Bi and 1-QL Bi<sub>2</sub>Te<sub>3</sub>. Dirac-cone states of Bi<sub>2</sub>Te<sub>3</sub> appear at about 0.2 eV below Fermi level (labeled by "D"). Fig. 5(f) presents the total spectra of 4-BL Bi. Obviously, no Dirac-cone states exist in Bi layers. From DFT calculations, we know the sharing of Dirac cone only exists in 1-BL Bi film.

In summary, we experimentally determined the low-energy electronic structures of ultrathin Bi(111) films grown on Bi<sub>2</sub>Te<sub>3</sub> ( $\leq 5$  BLs) with the help of DFT calculations. Bi(111) films we studied are all metallic. The compressed in-plane lattice constant increases the bandwidth of Bi(111) films' surface-state-like bands and changes their dispersions near the  $\bar{\Gamma}$  point. The strong hybridization between Bi and the Dirac-cone states in Bi<sub>2</sub>Te<sub>3</sub> observed in 1-BL film previously<sup>12</sup> do not occur in other thicknesses. On the other hand, the hybridization between Bi and Bi<sub>2</sub>Te<sub>3</sub>'s bulk states can extend spatially to 3 BLs from the interface.

This work is supported by National Basic Research Program of China (Grants No. 2012CB927401, No. 2011CB922200, No. 2013CB921902, and No. 2011CB921902), NSFC (Grants No. 11274228, No. 11174199, No. 11227404, No. 11374206, and No.

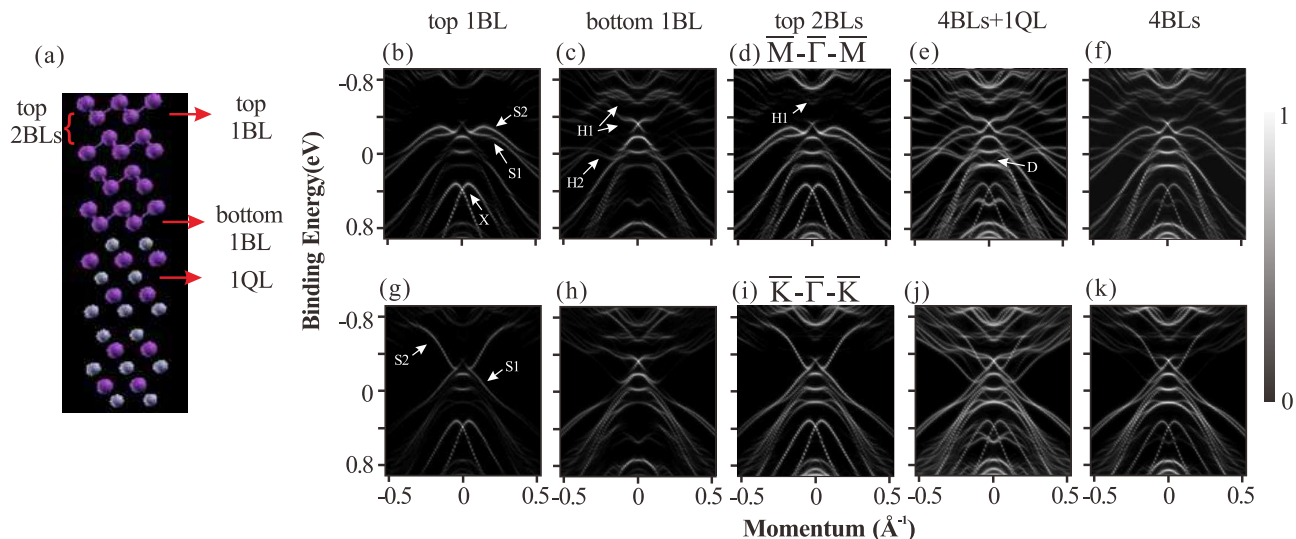


FIG. 5. (a) Side view of 4-BL Bi(111) film on  $\text{Bi}_2\text{Te}_3$ . The calculated spectra projected onto (b) top 1BL, (c) bottom 1BL, (d) top 2BLs, (e) 4BLs plus 1QL  $\text{Bi}_2\text{Te}_3$ (111) and (f) 4BLs along  $\bar{M}-\bar{\Gamma}-\bar{M}$  directions in 4-BL Bi(111)/ $\text{Bi}_2\text{Te}_3$ . The spectra caused by hybridization between Bi and  $\text{Bi}_2\text{Te}_3$  are marked by "H1" and "H2" in (c). The Dirac-cone surface states of  $\text{Bi}_2\text{Te}_3$  are marked by "D" in (e). (g-k) The calculated spectra projected onto the top 1BL, bottom 1BL, top 2BLs, 4BLs plus 1QL and 4BLs along  $\bar{K}-\bar{\Gamma}-\bar{K}$  directions.

11134008), Shanghai Committee of Science and Technology, China (Grants. No. 12JC140530 and No. 13QH1401500), C.L.G. acknowledges support from the Shu Guang project, which is supported by the Shanghai Municipal Education Commission and Shanghai Education Development Foundation. D.Q. acknowledges support from the Top-notch Young Talents Program and the Program for Professor of Special Appointment (Eastern Scholar). D.D.G acknowledges support from Open Research Fund Program of the State Key Laboratory of

Low-Dimensional Quantum Physics No. 14PJ1404600. The theoretical work conducted at University of Utah is supported by the office of Basic Energy Sciences, US Department of Energy Grant DE-FG02-04ER46148. We also thank the CHPC at University of Utah and NERSC for providing the computing resources. The Advanced Light Source is supported by the Director, Office of Science, Office of Basic Energy Sciences, of the U.S. Department of Energy under Contract No. DE-AC02-05CH11231.

\* dqian@sjtu.edu.cn

<sup>1</sup> P. Hofmann, Prog. Surf. Sci. **81**, 191 (2006).

<sup>2</sup> T. Hirahara, T. Nagao, I. Matsuda, G. Bihlmayer, E. V. Chulkov, Yu. M. Koroteev, P. M. Echenique, M. Saito, and S. Hasegawa, Phys. Rev. Lett. **97**, 146803 (2006).

<sup>3</sup> T. Hirahara, K. Miyamoto, I. Matsuda, T. Kadono, A. Kimura, T. Nagao, G. Bihlmayer, E. V. Chulkov, S. Qiao, K. Shimada, H. Namatame, M. Taniguchi, and S. Hasegawa, Phys. Rev. B **76**, 153305 (2007).

<sup>4</sup> T. Nagao, J. T. Sadowski, M. Saito, S. Yaginuma, Y. Fujikawa, T. Kogure, T. Ohno, Y. Hasegawa, S. Hasegawa, and T. Sakurai, Phys. Rev. Lett. **93**, 105501 (2004).

<sup>5</sup> Yu. M. Koroteev, G. Bihlmayer, E. V. Chulkov, and S. Blügel, Phys. Rev. B **77**, 045428 (2008).

<sup>6</sup> Z. Liu, C. Liu, Y. Wu, W. Duan, F. Liu, and J. Wu, Phys. Rev. Lett. **107**, 136805 (2011).

<sup>7</sup> Shuichi Murakami, Phys. Rev. Lett. **97**, 236805 (2006).

<sup>8</sup> M. Wada, S. Murakami, F. Freimuth, and G. Bihlmayer, Phys. Rev. B **83**, 121310 (2011).

<sup>9</sup> T. Hirahara, G. Bihlmayer, Y. Sakamoto, M. Yamada, H. Miyazaki, S. Kimura, S. Blügel, and S. Hasegawa, Phys.

Rev. Lett. **107**, 166801 (2011).

<sup>10</sup> F. Yang, L. Miao, Z. F. Wang, M. Y. Yao, F. Zhu, Y. R. Song, M. X. Wang, J. P. Xu, A. V. Fedorov, Z. Sun, G. B. Zhang, C. Liu, F. Liu, D. Qian, C. L. Gao, and J. F. Jia, Phys. Rev. Lett. **109**, 016801 (2012).

<sup>11</sup> Z.F. Wang, M. Y. Yao, W. Ming, L. Miao, F. Zhu, C. Liu, C.L. Gao, D. Qian, J. F. Jia, Naure Comm. **4**, 1384 (2013).

<sup>12</sup> L. Miao, Z. F. Wang, W. Ming, M. Y. Yao, M. X. Wang, F. Yang, F. Zhu, A. V. Fedorov, Z. Sun, C. L. Gao, C. Liu, Q. K. Xue, C. X. Liu, F. Liu, D. Qian, and J. F. Jia, Proc. Natl. Acad. Sci. USA **110**, 2758 (2013)

<sup>13</sup> T. Hirahara, N. Fukui, T. Shirasawa, M. Yamada, M. Aitani, H. Miyazaki, M. Matsunami, S. Kimura, T. Takahashi, S. Hasegawa, and K. Kobayashi, Phys. Rev. Lett. **109**, 227401 (2012).

<sup>14</sup> L. Miao, Z. F. Wang, M. Y. Yao, F. F. Zhu, J. H. Dil, C. L. Gao, C. H. Liu, F. Liu, D. Qian and J. F. Jia, Phys. Rev. B **89**, 155116 (2014).

<sup>15</sup> D.D. Reis, L. Barreto, M. Bianchi, G.A.S. Ribeiro, E.A. Soares, W.S. Silva, V.E. Carvalho, J. Rawle, M. Hoesch, C. Nicklin, W.P. Fernandes, J. Mi, B.B. Iversen, P. Hofmann,

Phys. Rev. B, **88**, 041404(R) (2013).

<sup>16</sup> M.Z. Hasan, C.L. Kane, Rev. Mod. Phys. **82**, 3045 (2010).

<sup>17</sup> I. K. Drozdov, A. Alexandradinata, S. Jeon, S. Nadj-Perge, H. Ji, R. J. Cava, B. A. Bernevig and Ali Yazdani, Nature

Phys. **10**, 663 (2014).

<sup>18</sup> G. Kresse and J. Hafner Phys. Rev. B **47**, 558 (1993).